

# Exploring the Mechanism of Yiwei Decoction in the Intervention of a Premature Ovarian Insufficiency Rat Based on Network Pharmacology and the miRNA-mRNA Regulatory Network

Weisen Fan, Hong Lei, Xuan Li, Yinghui Zhao, Yingjie Zhang,\* and Yalin Li



Cite This: *ACS Omega* 2024, 9, 19009–19019



Read Online

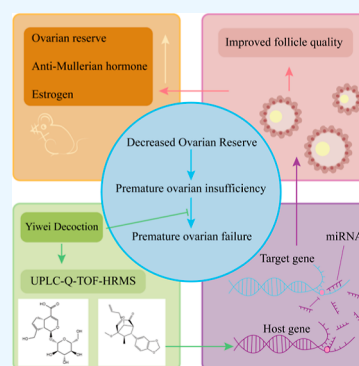
ACCESS |

Metrics & More

Article Recommendations

Supporting Information

**ABSTRACT:** Objective: our aim is to explore the mechanism of action of Yiwei decoction (YWD) in addressing premature ovarian insufficiency (POI) through a combination of transcriptomics and network pharmacology. By doing so, we hope to identify important pathways of action, key targets, and active components that contribute to the efficacy of YWD. Materials and Methods: group A comprised of the model + traditional Chinese medicine group, while group B was the model control group and group C was the normal control group. After gavage, serum AMH and E2 levels were measured by using ELISA. HE staining was used to study the impact of YWD on ovarian follicle recovery in POI rats. Additionally, RNA-seq sequencing technology was employed to analyze the transcription levels of mRNAs and miRNAs in the ovarian tissues of each group, and the resulting data were examined using R. YWD used UPLC-Q-TOF-HRMS to analyze its active ingredients. Upon obtaining the sequencing results, the miRWalk database was utilized to forecast the targets of DE miRNAs. Network pharmacology was then applied to predict the targets of active ingredients present in YWD, ultimately constructing a regulatory network consisting of active ingredients-mRNA-miRNA. The coexpression relationship between mRNAs and miRNAs was calculated using the Pearson correlation coefficient, and high correlation coefficients between miRNA-mRNA were confirmed through miRanda sequence combination. Results: the application of YWD resulted in improved serum levels of AMH and E2, as well as an increased number of ovarian follicles in rats with POI. However, there was a minimal impact on the infiltration of ovarian lymphocytes. Through GSEA pathway enrichment analysis, we found that YWD may have a regulatory effect on PI3K-Akt, ovarian steroidogenesis, and protein digestion and absorption, which could aid in the treatment of POI. Additionally, our research discovered a total of 6 DE miRNAs between groups A and B, including 2 new DE miRNAs. YWD contains 111 active compounds, and our analysis of the active component-mRNA regulatory network revealed 27 active components and 73 mRNAs. Furthermore, the coexpression network included 5 miRNAs and 18 mRNAs. Our verification of MiRanda binding demonstrated that 12 of the sequence binding sites were stable. Conclusions: our research has uncovered the regulatory network mechanism of active ingredients, mRNA, and miRNA in YWD POI treatment. However, further research is needed to determine the effect of the active ingredients on key miRNAs and mRNAs.



## 1. INTRODUCTION

The precise cause of premature ovarian insufficiency (POI) remains unknown, though it is believed to be influenced by a combination of genetic, immune, iatrogenic, and environmental factors.<sup>1</sup> Commonly observed clinical symptoms include abnormal menstruation, perimenopause, reproductive dysfunction, and perimenopause syndrome before the age of 40.<sup>2</sup> Unfortunately, the prevalence of this condition is increasing annually. While hormone therapy can alleviate abnormal menstruation and perimenopause symptoms, it does not address patients' ovarian reserves, making it insufficient in treating this disease.<sup>3</sup> To truly enhance the physical and mental wellbeing of patients, particularly those with fertility concerns, it is necessary to improve their ovaries' reproductive function.<sup>4</sup>

Traditional Chinese medicine (TCM) is an effective treatment for POI with minimal side effects. Acupuncture and Chinese herbal therapy have been shown to reduce follicle-

stimulating hormone and increase estrogen levels in patients.<sup>5–7</sup> Yiwei decoction (YWD), a classic prescription for female aging, can improve reproductive function and delay the aging process by tonifying Yangming Fluid and Qi. Many of the ingredients in YWD have antiaging and antioxidant properties. Previous studies have demonstrated that YWD improved ovarian reserve, decreased FSH, and increased estradiol levels in POI patients.<sup>8</sup> Additionally, YWD reduced granulosa cell apoptosis in primary senile female rats, enhanced granulosa cell mitochondria, and regulated neuroendocrine

**Received:** November 30, 2023

**Revised:** March 29, 2024

**Accepted:** April 3, 2024

**Published:** April 17, 2024



function.<sup>9,10</sup> Despite conducting a thorough analysis, the exact way that YWD intervention affects POI remains unclear. MiRNAs, a type of naturally occurring small RNA between 20 and 24 nucleotides in length, can regulate a single gene with the help of multiple miRNAs.<sup>11</sup> Extensive research has demonstrated the crucial role miRNA plays in the development and treatment of POI.<sup>12</sup> Consequently, this study aims to investigate the mechanism behind YWD intervention in POI rats through the lens of miRNA-mRNA regulatory network and network pharmacology, with the goal of identifying active ingredients and uncovering the intervention's action mechanism.

## 2. MATERIALS AND METHODS

**2.1. Reagents and Experimental Animals.** The experiment was approved by the Animal Ethics Committee of Shandong University of TCM and certified by the Institutional Review Board of the Affiliated Hospital of Shandong University of TCM. It was confirmed that the study did not involve human ethics and did not require any approval of human ethics. The study used 45 eight-week-old female SD rats provided by Beijing Vitonglihua Experimental Animal Technology Co., Ltd. The rats were adaptively fed for 1 week after entering the barrier environment, and the rat maintenance feed (10 kg/bag) was provided by Beijing Keao. After staining the rats' vaginal smears with the crystal violet staining method and observing them for 10 days, 45 rats were randomly assigned to three groups (A, B, and C) after confirming a normal estrous cycle for each rat.

In the conducted study, we assigned one group as the control (group C), while groups A and B were subjected to cyclophosphamide (CTX) treatment for inducing modeling (source leaf: BYBZ30088). The initial dosage of CTX was 50 mg/kg, followed by a maintenance dose of 8 mg/kg/d for 14 days.<sup>13</sup> In contrast, group C received a comparable amount of normal saline. Postmodeling, we used crystal violet staining to observe the estrous cycle of each group for 10 days (source leaf: BYBZ14829). We can confidently say that the modeling was successful as the rats' estrous cycle deviated from normal for ten consecutive days.

**2.2. Experimental Animals and Specimens Collection.** The Pharmacy Department of Shandong University of Chinese Medicine's Affiliated Hospital provided intragastric Chinese herbs. Composition of the drug: *Glehnia littoralis* 18 g, *Ophiopogon japonicus* 30 g, *Rehmannia glutinosa* 30 g, and *Polygonatum odoratum* 9 g. MPNS (<http://mpns.kew.org>) verified all drug names. The herbal compound was concentrated at 100 mL, and the drug concentration was 0.87 g/mL. The dose of YWD for rats should be 7.830 g/kg/d, according to the equivalent dose ratio table of human and animal body surface area. Groups A and B received gavage for YWD, while group C received gavage with an equal volume of normal saline for 4 weeks. All rats were sedated for 5 min by inhaling 2% isoflurane[] (Ryward: HYT11281368). For 5 min, rats were sedated with 3% isoflurane (Ryward: HYT11281368), followed by 1.5% maintenance anesthesia. Each group's abdominal aorta blood and ovaries were taken after anesthesia. After sampling, the rats were slaughtered by decapitation while being anesthetized.

**2.3. HE Stains.** To prepare the ovaries for further analysis, they were first fixed in a 4% paraformaldehyde solution (refer to document BYBZ14586). Next, the tissue was cut to approximately 3 mm thickness in order to undergo

dehydration and paraffin embedding. 4 mm thick paraffin sections were then created and stained with hematoxylin (Solarbio: G1142) for 5 min to highlight the cell nucleus, followed by a 3 min eosin (Solarbio: XY21114937) staining to highlight the cytoplasm. Finally, the sections were dehydrated and sealed for preservation.

**2.4. Transcriptomic Analysis.** **2.4.1. Extraction of RNA.** Total RNA was extracted from the tissue using RNA Purification Reagent (Invitrogen) as directed by the manufacturer, and genomic DNA was removed using rDNase I RNase-free (TaKara). The ND-2000 and a 2100 Bioanalyzer (Agilent Technologies, Santa Clara, CA, USA) were used to assess RNA quality (NanoDrop Technologies). To build the sequencing library, only high-quality RNA samples (OD260/280 = 1.8–2.2, OD260/230  $\geq$  2.0, RIN  $\geq$  8, 28S:18S  $\geq$  1.0, > 10  $\mu$ g) were used.

**2.4.2. Library Preparation.** The RNA-seq transcriptome strand library was prepared using 5 g of total RNA using the Illumina's TruSeq™ stranded total RNA Kit (San Diego, CA). To summarize, the Ribo-Zero Magnetic kit was used to deplete rRNA instead of poly(A) purification and then fragmented by fragmentation buffer first. Then, using random hexamer primers, first-stranded cDNA was synthesized. The RNA template was then removed, and a replacement strand was synthesized with dUTP instead of dTTP to generate ds cDNA. Because the polymerase did not incorporate beyond this nucleotide, the incorporation of dUTP quenched the second strand during amplification. The ds cDNA was separated from the second strand reaction mix using AMPure XP beads. To prevent these blunt fragments from ligating to one another during the adapter ligation reaction, a single 'A' nucleotide was added to the 3' ends. Finally, the ends of the ds cDNA were ligated with multiple indexing adapters. On 2% Low Range Ultra Agarose, libraries were size selected for cDNA target fragments of 200–300 bp and then PCR amplified for 15 PCR cycles with Phusion DNA polymerase. Following TBS380 quantification, the paired-end RNA-seq sequencing library was sequenced with the Illumina HiSeq xten/NovaSeq6000 (2  $\times$  150 bp read length). Furthermore, Truseq™ Small RNA sample prep Kit was used to ligate 3  $\mu$ g of total RNA with sequencing adapters (Illumina, San Diego, CA, USA). Following that, cDNA was synthesized via reverse transcription and amplified via 12 PCR cycles to create the libraries. Deep sequencing was performed by Shanghai Majorbio Bio-Pharm Biotechnology Co., Ltd. after TBS380 quantification (Shanghai, China).

**2.4.3. Transcriptome Assembly and Read Mapping.** The raw paired end reads were trimmed and quality controlled using the default parameters of SeqPrep (<https://github.com/jstjohn/SeqPrep>) and Sickle (<https://github.com/najoshi/sickle>). The clean reads were then aligned to the reference genome in orientation mode using the HIASAT<sup>14</sup> software (<https://ccb.jhu.edu/software/hisat2/index.shtml>). StringTie (<https://ccb.jhu.edu/software/stringtie/index.shtml?t=example>) was used to assemble the mapped reads of each sample using a reference-based approach.<sup>15</sup>

**2.4.4. MiRNAs Identification.** Low-quality bases (Sanger base quality of 20) from the 3' end were trimmed using in-house perl scripts, and the sequencing adapters were removed using the fastx toolkit software (<http://hannonlab.cshl.edu/fastxtoolkit/>). All identical sequences with lengths ranging from 18 to 32 nt were counted and removed from the initial data set. To remove non-miRNAs sequences, the assembled

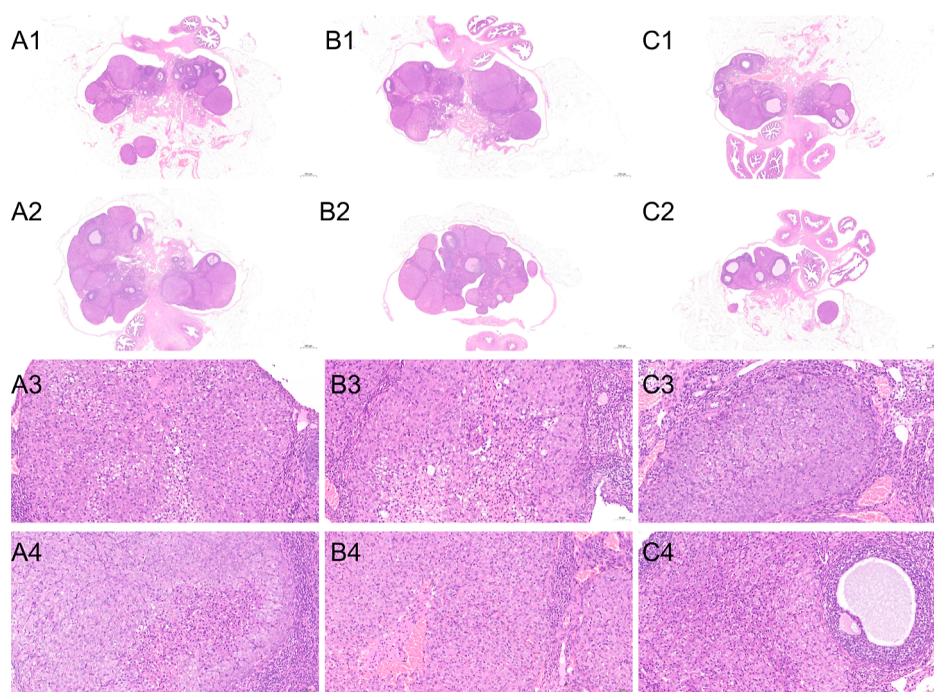


**Figure 1.** Groups A and C had significantly more follicles than group B. There was no obvious lymphocyte infiltration in group C's ovarian tissue, but there was some in group B and a small amount in group A.

unique sequences were BLAST searched against the Rfam database, version 10.1 (<http://rfam.sanger.ac.uk/>) (rRNA, tRNA, snoRNA, etc.). Bowtie was used to annotate the chromosomal location against the reference genome data (<http://bowtie-bio.sourceforge.net/index.shtml>). The perfectly matched sequences were used to count and analyze the known miRNAs expression profile using a BLAST search of the miRbase, version 21.0 (<http://www.mirbase.org/>). The hairpin structure of miRNAs precursors can be used to predict novel miRNAs. To predict novel miRNAs, the available software mireap was integrated. Simultaneously, in-house scripts were used to obtain the identified miRNA base bias on the first position with a specific length as well as on each position of all identified miRNAs. The transcript per million read (TPM) method was used to calculate the expression level of each miRNA.

**2.4.5. Analysis of Differential Expression.** The expression level of each transcript was calculated using the TPM method to identify differential expression of mRNAs (DEmRNAs) and miRNAs (DEmiRNAs) between two different samples. To calculate gene abundances,<sup>16</sup> RSEM (<http://deweylab.biostat.wisc.edu/rsem/>) was used. DEseq2<sup>17</sup> was used to extract significantly DEmiRNAs and DEmRNAs with  $\log_2FCI > 1$  and  $p$ -value  $< 0.05$ .

**2.5. ELISA Examination.** Six samples of abdominal aortic blood were randomly selected from each of the three groups and placed in a centrifuge tube to naturally coagulate at room temperature for 15 min. After centrifugation at 3000 rpm for 20 min, the supernatant was collected. Follow the merchant's instructions to complete the detection of antimüllerian hormone (AMH) and E2.

**2.6. UPLC-Q-TOF-HRMS.** The experiment was carried out using a Waters HClass instrument with a mobile phase consisting of 0.1% formic acid (A) and formic acid acetonitrile (B) and a Waters BEH C18 (1.7  $\mu\text{m}$  2.1  $\times$  50 mm) chromatographic column. The gradient elution protocol

involved the following steps: 0–2 min at 95% A; 2–30 min at 95% A to 2% A; 30–35 min at 2% A; 35–39 min at 2% A to 95% A; 39–40 min at 95% A; 0–2 min at 5% B; 2–30 min at 5% B to 98% B; 30–35 min at 98% A; 35–39 min at 98% A to 5% A; and 39–40 min at 5% A. The column was kept at a temperature of 40 °C, and the flow rate was set at 0.4 mL/min, with an injection volume of 3  $\mu\text{L}$ .

For the mass spectrometry analysis, we utilized a Waters G2-XS Qtof instrument and employed both positive and negative ion modes for detection. The mass scanning range was set between  $m/z$  50–1200, with a spray voltage of 4500 V<sup>18</sup> and an ion source temperature of 110 °C. Collision energy was adjusted between 20 and 40 V, and the nitrogen flow rate was maintained at 800 L/h. The desolvation temperature was set at 400 °C to ensure accurate results.

**2.7. Network Pharmacology.** To create an active ingredient–target map for Chinese herbs, we utilized the TCMSP database (<https://old.tcmsp-e.com/tcmsp.php>)<sup>19</sup> to select active ingredients. From there, we identified the corresponding targets and removed any duplicates. The resulting targets were then cross-referenced with the targets of POI in the Gene Cards database (<https://www.genecards.org/>).

**2.8. Data Analysis.** Volcanic maps were used to map DEmRNAs between groups A and B, while heat maps were utilized to represent all DEmiRNAs. To further screen significant DEmRNAs, a  $P$ -adjust  $< 0.05$  was set and indicated by a heat map. GSEA pathway analysis enriched meaningful pathways between AvsB and BvsC, with curve images illustrating changes in their intersection pathways.

We predicted targets of DEmiRNAs between groups A and B using the miRWalk<sup>20</sup> database (<http://mirwalk.umm.uni-heidelberg.de/>). To visualize the relationship between active ingredients–mRNA–miRNA, we utilized Cytoscape 3.8.2 based on the intersection of mRNA of predicted targets of YWD and DEmiRNAs and DEmRNAs. The Pearson correlation

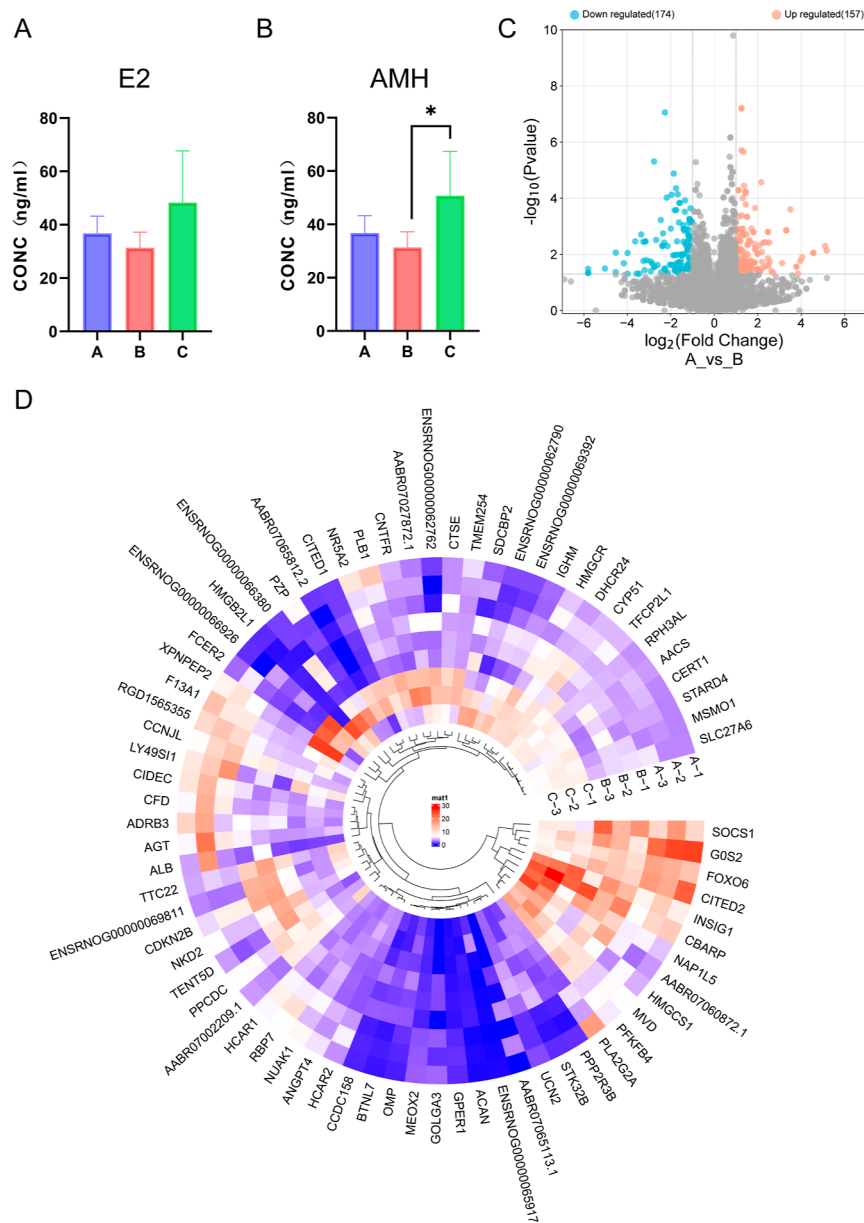


**Figure 2.** A represents the E2 level in rat serum, while B represents the AMH level in rat serum. Group C had the highest E2 and AMH levels, while Group B had the lowest. C denoted DE mRNAs in A vs B ( $P < 0.05$ ), light blue denoted genes that were down-regulated in group A compared to group B, and light orange denoted the opposite. D represented all A vs B, B vs C, and A vs C high-significance DE mRNAs expression ( $P$ -adjust  $< 0.05$ ), with red representing high expression and blue representing low expression.

coefficient was implemented to calculate the coexpression relationship between mRNA and miRNA in groups A and B. After screening high confidence miRNA-mRNA relationships, we created a network map. To calculate the sequence binding sites and energies of these miRNA-mRNAs, we utilized MiRanda 3.3a.<sup>21</sup>

### 3. RESULTS

**3.1. Ovarian Function and Tissue.** The results depicted in Figure 1 demonstrate that there were significantly more follicles in ovarian tissue from groups A and C in comparison to those from group B. Despite this, groups A and B still displayed lymphocyte infiltration, while group C did not show any apparent signs of infiltration. This indicates that YWD may improve ovarian reserve in cases of POI, but may not have a substantial impact on chronic tissue inflammation. Further-

more, as illustrated in Figure 2 by A and B, AMH and E2 values were higher in group A than in group B, but still lower than those in group C. These findings suggest that YWD may have therapeutic benefits in treating POI caused by CTX, ultimately restoring ovarian reserve and function.

**3.2. MRNAs and miRNAs Differential Expression Analysis.** Our study revealed the presence of 679 DE mRNAs ( $P < 0.05$ ), with 331 DE mRNAs observed between A vs B. Notably, 74 DE mRNAs had a high significance level ( $P$ -adjust  $< 0.05$ ). For a more comprehensive picture, refer to Figure 2C,D. Supporting Information 1 provides detailed information about mRNA expression levels. Our results from the GSEA pathway enrichment analysis indicated that CTX-induced POI rats experienced significant down-regulation in the PI3K-Akt, tuberculosis, protein digestion and absorption, ovarian steroidogenesis, ECM-receptor interaction, phagosome, and

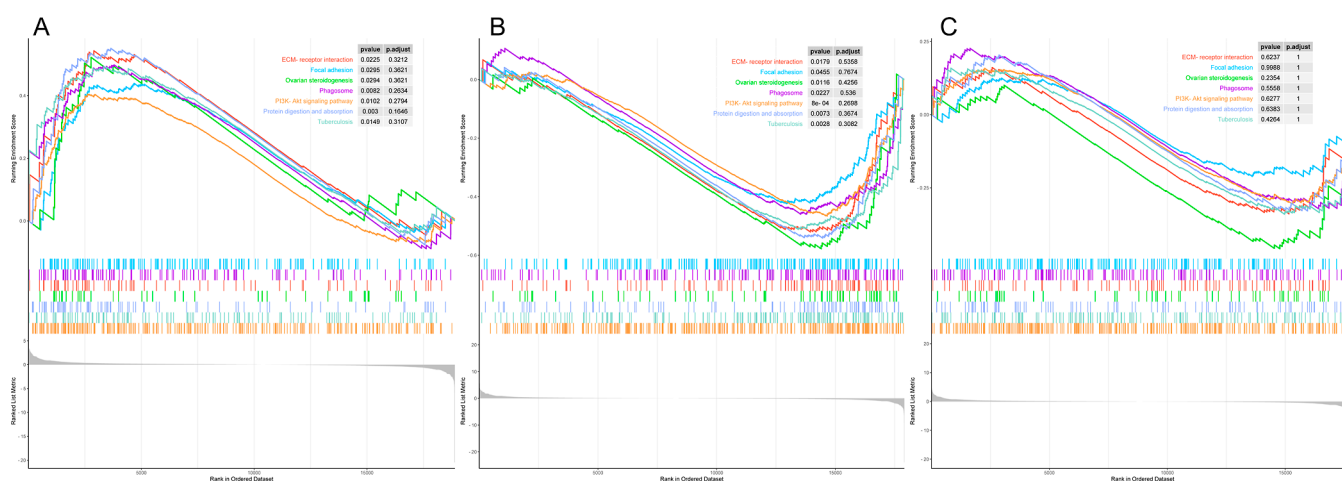


**Figure 3.** GSEA pathway enrichment map revealed that A vs B and B vs C shared significant pathways ( $P < 0.05$ ). The path is represented by the color of the curve, with a curve above 0 representing an up-regulated pathway and a curve below 0 representing a down-regulated pathway. Seven pathways were up-regulated when compared to groups A and B; seven pathways were down-regulated when compared to groups B and C; and seven pathways were down-regulated when compared to groups A and C, but there was no statistical significance.

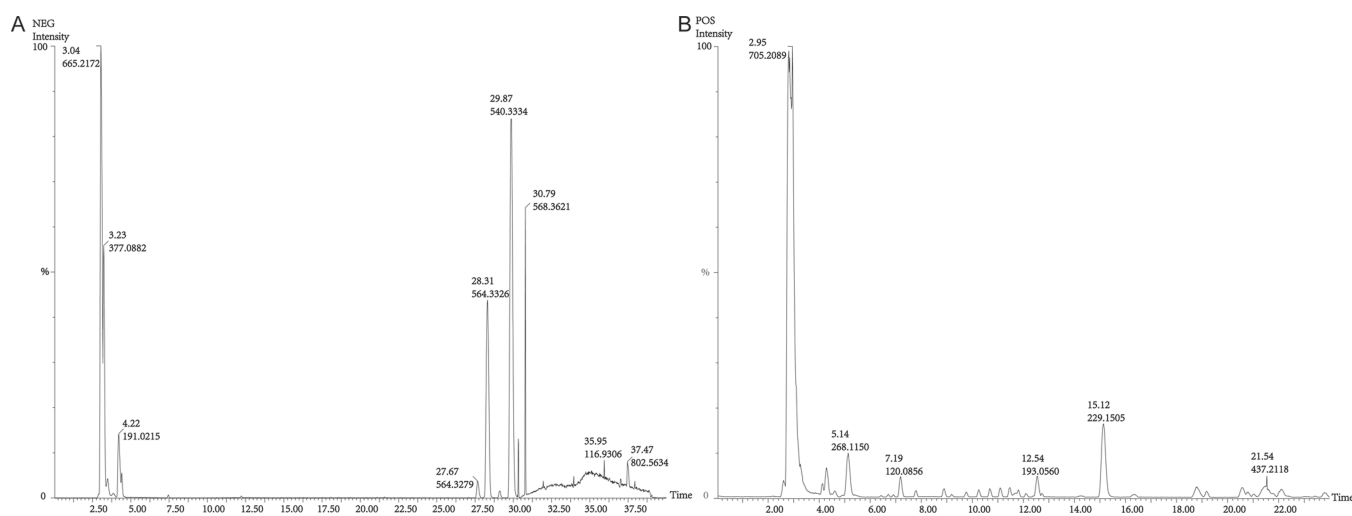


**Figure 4.** Negative mode of the liquid-mass map is represented by A, The positive mode of the liquid-mass map is represented by B. Time and peak are indicated by the numbers given for each peak.

focal adhesion pathways, relative to normal rats. However, we found that YWD treatment can up-regulate these pathways, thereby treating POI and restoring ovarian function. Figure 3 contains additional information about this finding. Additionally, our study uncovered 11 DEMiRNAs ( $P < 0.05$ ), with 6 identified between AvsB. For more information, please refer to Figure 5A,B. Supporting Information 2 provides detailed information on miRNA expression levels.

**3.3. Identification of YWD's Active Components.** After detecting UPLC-Q-TOF-HRMS,<sup>22</sup> we retrieved the Waters UNIFI TCM database. The results, depicted in Figure 4, revealed 8 active components in the negative mode and 103 active ingredients in the positive mode. For the full composition, please refer to Supporting Information 3. We then narrowed it down to 27 active compounds after searching the TCMSP database, and the details can be found in Table 1.

**3.4. Establishment of a miRNA-mRNA-Active Ingredients Network.** By exploring a database, it was uncovered that groups A and B had 248 targets of action for DEMiRNAs, while the 27 active components combined had 126 targets. The intersection of targets and DEMiRNAs is visible in Figure

5C. To identify targets linked to diseases, the GeneCards database was consulted, revealing 5044 disease-related targets. Of these, 77 were shared between illness targets and targeting targets. PTGS2 emerged as the most frequently targeted active ingredient intervention. Further details can be found in Figure 6A. To construct the active ingredients-mRNA-miRNA regulatory network, 36 mRNAs intersecting with AvsB's mRNAs were used. As depicted in Figure 6B, the targets coregulated by miRNAs and active ingredients were RELA and MMP2.

**3.5. Establishment of a Network of miRNA-mRNA Coexpression.** The coexpression relationship between AvsB DEMiRNAs and high-significance AvsB DEMiRNAs ( $P$ -adjust  $< 0.05$ ) was calculated using the Pearson correlation coefficient. As illustrated in Figure 7, Cytoscape3.8.2 was utilized to showcase 46 expression relationships of significance ( $P < 0.05$ ). MiRanda3.3a was configured with score = 140 and energy = -1, resulting in six dependable miRNA-mRNA sequences. Among these sequences, there are 5 binding sites for miR-3102-ACAN and 3 binding sites for miR-187-3p-ACAN. Additional details can be found in Figure 8.

Table 1. TCMSP Database Contains the Target's Active Component

identification	formula	$t_R$ /min	response value	$m/z$	error/ppm	adduct
geniposidic acid	C16H22O10	2.87	5443	375.1275	-2.8	+H
L-glutamic acid	C5H9NO4	3.13	2165	148.0619	9.9	+H
O-aminobenzoic acid	C7H7NO2	3.14	2015	138.0561	8.5	+H
interiotherin A	C29H28O8	3.27	6724	505.1850	-1.4	+H
mangiferin	C19H18O11	3.32	2095	423.0910	-2.9	+H
L-Arg	C6H14N4O2	3.94	19089	175.1199	5.4	+H
L-tyrosine	C9H11NO3	4.49	7394	182.0828	8.9	+H
O-coumaric acid	C9H8O3	4.53	10407	165.0560	8.2	+H
adenosine	C10H13NSO4	5.14	67777	268.1051	4.2	+H
phenylalanine	C9H11NO2	7.19	7926	166.0874	7	+H
3- <i>n</i> -butylphthalide	C12H14O2	17.15	5139	191.1063	-1.7	+H
umbelliferone	C9H6O3	18.80	21620	163.0399	5.6	+H
scopoletin	C10H8O4	19.13	2753	193.0509	7.3	+H
vomifoliol	C13H20O3	22.18	4866	225.1499	6.3	+H
uridine	C9H12N2O6	23.43	4151	245.0789	8.7	+H
cniforinB	C23H26O7	23.90	6233	415.1736	-3.6	+H
schisantherin A	C30H32O9	23.97	6037	537.2109	-1.9	+H
oxyphyllendiola	C14H22O3	25.45	3056	239.1630	-4.8	+H
kadsureninB	C20H22O5	26.01	3283	343.1548	2.5	+H
isolinderoxide	C16H20O2	26.28	3425	245.1527	-3.8	+H
kurarinone	C26H30O6	29.11	2276	439.2105	-2.4	+H
schisandrin A	C24H32O6	29.11	3593	417.2274	0.6	+H
linolenic acid	C18H30O2	29.24	2772	279.2332	4.9	+H
dibutyl phthalate	C16H22O4	30.43	5318	279.1601	3.5	+H
Gingerol	C17H26O4	30.59	5978	295.1888	-5.2	+H
vitetrifolinE	C22H36O4	32.27	4467	365.2675	-3	+H
mulberofuran A	C25H28O4	38.83	6481	393.2090	7.5	+H

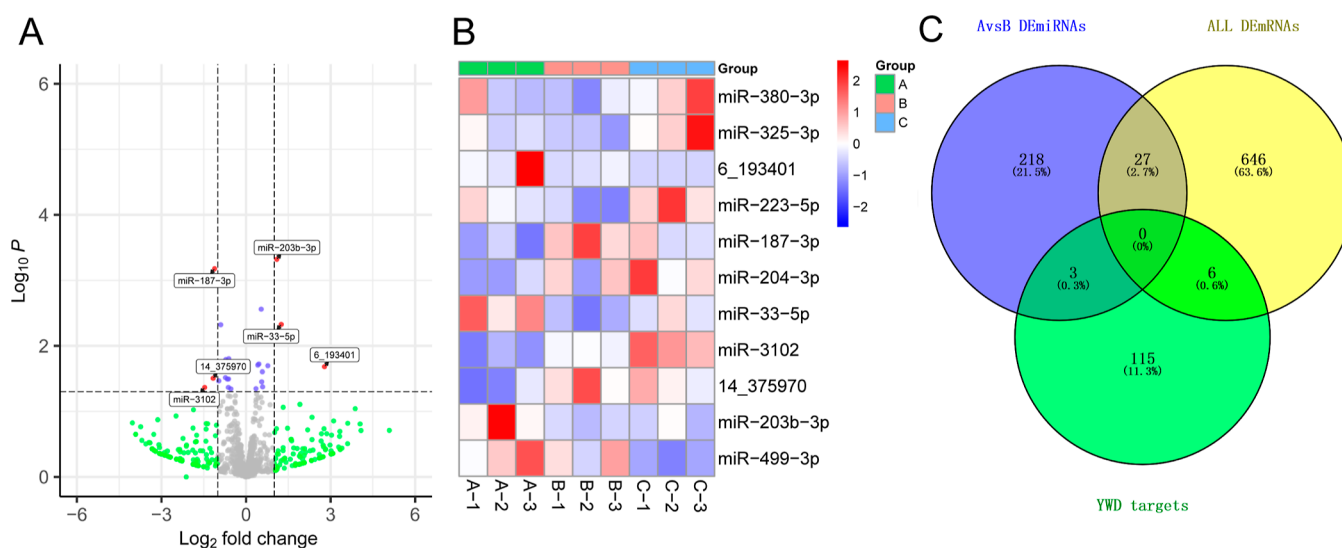


**Figure 5.** A represents 6 DE miRNAs in A vs B, three up and three down. B represents all A vs B, B vs C, and A vs C DE miRNAs, with red indicating high expression and blue indicating low expression. C is the intersection target of the YWD target, the DE miRNAs of A vs B, and the miRNAs target. YWD and DE miRNAs regulated a total of 33 A vs B DE miRNA targets.

#### 4. DISCUSSION

YWD comprises four Chinese herbs that possess potent antiaging and antioxidant properties with potential to counteract reproductive aging. Raw *R. glutinosa* contains Rehmanniol, which effectively inhibits plasma protein oxidation induced by  $H_2O_2/Fe$  and inhibits superoxide anion production in resting platelets when extracted at 50g/mL.<sup>23</sup> *Ophiopogon japonicus* and *G. littoralis* contain stigmasterol and uridine, which can enhance antioxidant enzyme activity and SOD levels in the

serum and brain tissue of cerebral ischemia-reperfusion model rats, while also slowing the aging of the intestine by decreasing inflammation and oxidative stress.<sup>24,25</sup> Additionally, quercetin found in *G. littoralis* increases glutathione levels, strengthens the body's antioxidant defense system, and lowers ROS levels.<sup>26</sup> Finally, Polygonatum odoratum contains oleic acid, which regulates metabolic enzyme activity and antioxidant defense systems to reduce endogenous ROS production.<sup>27</sup> Other key ingredients in YWD include O-coumaric acid,<sup>28</sup> L-

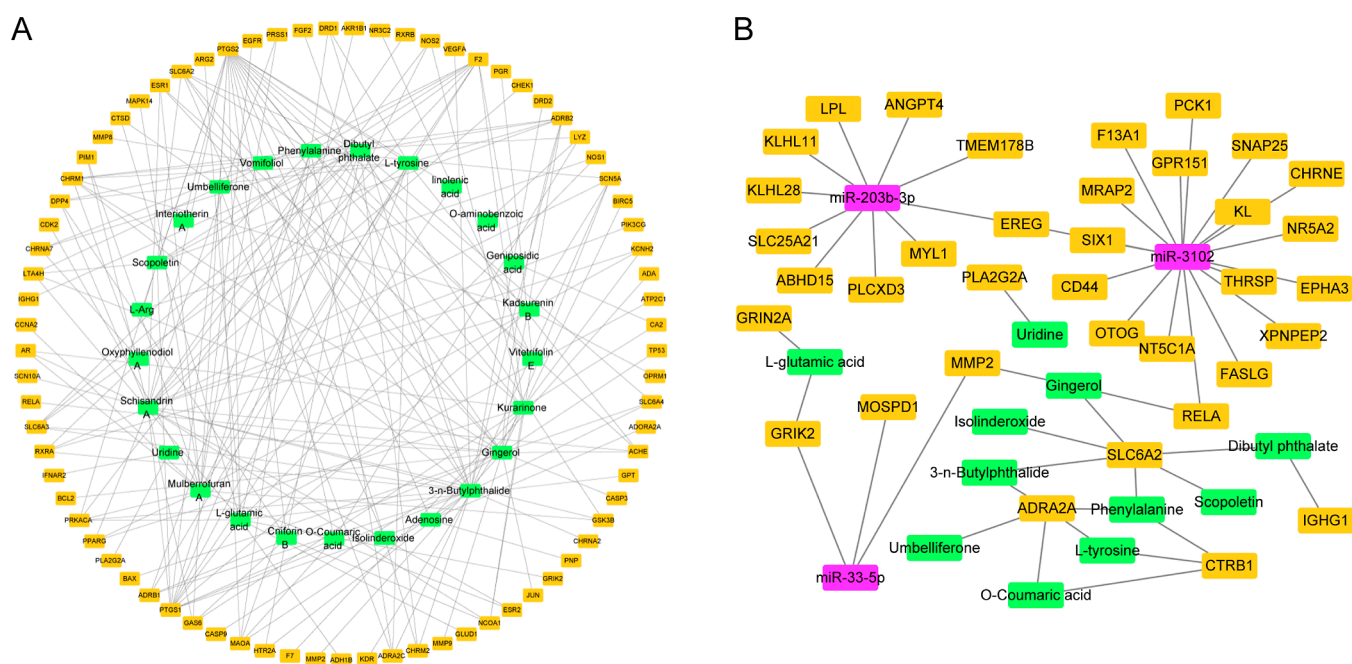


**Figure 6.** Active ingredient and target network diagram is represented by A. The intersecting targets are represented by orange, the 27 TCM active ingredients that have been identified are represented by green, and the associations between the active ingredient and the target are shown by gray lines. The active ingredient-miRNA network diagram is shown by B. The active component of YWD is shown by green, DEmiRNAs by orange, and DEmiRNAs by purple.

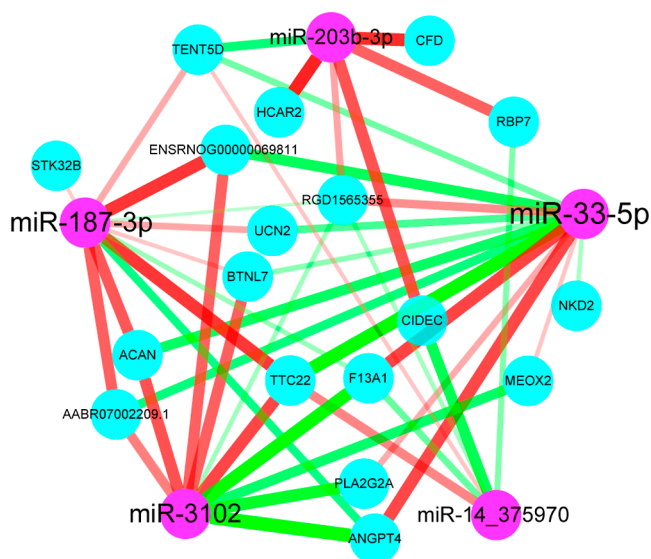


**Figure 7.** Purple represents miRNA, blue represents mRNA, and the connection lines represent the *P* value and correlation coefficient. The red line represents a positive correlation, while the green line represents a negative correlation. The lower the *P* value and the more reliable the connection, the thicker the connection line. The stronger the correlation, the darker the connection line color.

glutamic acid,<sup>29</sup> umbelliferone,<sup>30</sup> and schisandrin A,<sup>31</sup> all of which possess potent antioxidant properties.

Currently, the method by which TCM compounds treat diseases is not fully understood. The active ingredients in Chinese herbs often have an indirect effect on gene expression through noncoding RNA.<sup>32</sup> To shed light on this, we investigated how YWD treatment affects the regulatory mechanism of POI via the active component-mRNA-miRNA regulatory network. Figure 5A demonstrates that YWD

intervention in POI rats can boost the expression of miR-203-3p and miR-33-5p while reducing the expression of miR-3102 and miR-187-3p in the ovarian tissue. While there is no direct evidence linking these DEmiRNAs to follicular development, they appear to play a role in cell proliferation and apoptosis. For instance, miR-33-5p has been found to ease spinal cord injury in rats and reduce apoptosis in lipopolysaccharide-induced PC12 cells.<sup>33</sup> Additionally, miR-33-5p has been observed to boost osteoblast activity and mineralization in vitro, and targeted delivery of miR-33-5p has been suggested as a possible treatment for pathological bone loss, providing a potential avenue for future research into the YWD treatment of POI-induced osteoporosis. MiR-203b-3p and miR-187-3p are frequently studied for their anticancer properties. For instance, miR-203b-3p<sup>34</sup> has been shown to suppress the proliferation and invasion of rectal cancer cells, while miR-187-3p<sup>35</sup> has been found to inhibit the proliferation and migration of nonsmall cell lung cancer cells and promote apoptosis by targeting the oncogene BCL6.

Based on the research findings illustrated in Figure 6A, PTGS2 appears to be the primary target of the active components. In the pathophysiology of POI, PTGS2 plays a critical role, as it can trigger inflammation and cell death.<sup>36</sup> TCM may be able to treat ovarian dysfunction by regulating PTGS2 expression.<sup>37</sup> Mantawy<sup>38</sup> et al. found that chrysin reduced PTGS2 levels and restored estradiol levels in the ovaries of rats with ovarian failure. In POI rats, RELA, another important gene associated with inflammation, is often overexpressed. By controlling this target, resveratrol intervention might help restore ovarian function in POI rats.<sup>39</sup> MMP2 is a key target of fibrosis, which is associated with the fibrosis process of many human tissues. Although there is no evidence linking pathological fibrosis alterations in ovarian tissue of POI patients to MMP2, follicular development and MMP2 are closely related.<sup>40,41</sup> When ovarian tissue has a high



**Figure 8.** In the miRNA-mRNA sequence binding diagram, the red letters represent the base complementation of the junction points, Energy represents the energy required for miRNA to bind to mRNA, and mRNA position represents the position on the gene sequence where miRNA acts. "|" represents the hydrogen bond, and ":" represents the two hydrogen bonds.

expression of MMP2, follicles are vulnerable to atresia, which may explain the aberrant follicular formation observed in POI patients.

CTX is widely utilized chemotherapy in clinical settings. It has the potential to decrease AMH and E2 levels by damaging DNA, hindering RNA and protein formation, and harming primary follicles and granulosa cells.<sup>42,43</sup> Our findings indicate that CTX significantly reduced ovarian steroidogenesis, PI3K-Akt, and focal adhesion pathways in group B rats. PI3K-Akt inhibits apoptosis,<sup>44</sup> and when serum Resistin studies ovarian tissue, it triggers the PI3K-Akt pathway and prevents ovarian cell apoptosis.<sup>45</sup> The ovarian steroidogenesis pathway is vital to E2 and P production and is a crucial ovarian reproductive function. The disruption of this pathway suggests that CTX impairs ovarian hormone synthesis.<sup>46</sup> The focal adhesion pathway is linked to granulosa cell differentiation, apoptosis, and adhesion. The focal adhesion kinase, the activator of the focal adhesion pathway, is also linked to follicle development.<sup>47</sup> Various species studies have shown that the ECM-receptor interaction pathway is also involved in follicle development

and maturation, and that its multiple molecules can reflect follicle quality.<sup>48–50</sup> As demonstrated in Figure 3A,C, YWD treatment effectively restored abnormal pathways in rats, suggesting that it may have therapeutic effects by regulating these pathways.

The coexpression of miRNAs and mRNAs may allow for the prediction of miRNA targets and reveal the molecular mechanisms of YWD treatment for POI. Figure 7 displays the reliable miRNA-mRNA pairs such as miR-187-3p-TTC22, miR-187-3p-ACAN, miR-203b-3p-HCAR2, miR-33-5p-ANGPT4, and others. From our sequence binding verification, we identified ANGPT4, F13A1, ACAN, TENT5D, and STK32B as the most probable targets of DEmiRNAs. ANGPT4, for instance, could be a candidate growth factor that regulates ovarian function by promoting endothelial cell survival, migration, and angiogenesis through cell-cell interactions.<sup>51,52</sup> Our base complementation analysis showed that ANGPT4 interacts with miR-187-3p. Since ANGPT4 is an angiogenic factor, YWD has the potential to increase its expression and restore ovarian function in the treatment of

POI by upregulating the production of angiogenic factors and improving ovarian blood flow. However, more research is needed to confirm their respective roles in ovarian function restoration. There is a strong correlation between F13A1 and recurrent abortion. In mature bovine follicle follicular fluid, F13A1 expression was observed to be higher than in immature bovine follicle follicular fluid.<sup>53,54</sup> ACAN is known to be down-regulated in the adipose tissue of patients with polycystic ovary syndrome.<sup>55</sup> TENTSD mutations may lead to male infertility, while TENTSD deficiency can interfere with mRNA stability during spermatogenesis and cause male infertility.<sup>56,57</sup>

## 5. CONCLUSIONS

In this study, we were able to determine how YWD affects POI rats by analyzing miRNA and mRNA levels. Through this analysis, we uncovered an active ingredient-mRNA-miRNA regulation network that targets RELA, EREG, and MMP2. By upregulation of PI3K-Akt, protein digestion and absorption, and ovarian steroidogenesis, YWD has the potential to restore ovarian function. Our research also identified potential targets of DEmiRNAs, including F13A1, ACAN, TENTSD, and STK32B, through a miRNA-mRNA coexpression network. While further investigation is needed to fully understand the effects of these targets, our findings provide a solid groundwork for future research.

## ■ ASSOCIATED CONTENT

### Data Availability Statement

The data is available throughout the manuscript and supporting files.

### SI Supporting Information

The Supporting Information is available free of charge at <https://pubs.acs.org/doi/10.1021/acsomega.3c09551>.

- mRNA transcriptome data of rats in each group (XLS)
- miRNA transcriptome data of rats in each group (XLS)
- Compounds in YWD detected by HPLC-Q-TOF-HRMS (XLS)

## ■ AUTHOR INFORMATION

### Corresponding Author

**Yingjie Zhang** – *The First Clinical College of Medicine, Shandong University of Traditional Chinese Medicine, Jinan 250013, China*; [orcid.org/0000-0002-2181-1617](https://orcid.org/0000-0002-2181-1617); Email: [2021111031@sduatcm.edu.cn](mailto:2021111031@sduatcm.edu.cn)

### Authors

**Weisen Fan** – *The First Clinical College of Medicine, Shandong University of Traditional Chinese Medicine, Jinan 250013, China*

**Hong Lei** – *The First Clinical College of Medicine, Shandong University of Traditional Chinese Medicine, Jinan 250013, China*

**Xuan Li** – *The First Clinical College of Medicine, Shandong University of Traditional Chinese Medicine, Jinan 250013, China*

**Yinghui Zhao** – *College of Traditional Chinese Medicine, Shandong University of Traditional Chinese Medicine, Jinan 250013, China*

**Yalin Li** – *The First Clinical College of Medicine, Shandong University of Traditional Chinese Medicine, Jinan 250013, China*

Complete contact information is available at:

<https://pubs.acs.org/10.1021/acsomega.3c09551>

## Author Contributions

WeiSen Fan and Hong Lei conceived and designed the experiment and wrote the manuscript. Xuan Li is responsible for animal feeding and indicator monitoring. Yingjie Zhang was responsible for the proofreading and data analysis of the article. Yinghui Zhao and Yalin Li were responsible for the experimental pictures and literature search. All authors read and approved the final manuscript.

## Funding

This research was supported by the Natural Science Foundation of Shandong Province (ZR2021MH404).

## Notes

The authors declare no competing financial interest.

## ■ ACKNOWLEDGMENTS

All animal use has been approved by the Animal Welfare Ethics Review Committee of Shandong University of Traditional Chinese Medicine with the approval number SDUTCM20210224024.

## ■ ABBREVIATIONS

- YWD, Yiwei decoction
- POI, premature ovarian insufficiency
- TCM, premature ovarian insufficiency
- E2, estradiol
- CTX, cyclophosphamide
- TPM, transcripts per million
- DEmRNAs, differential expression mRNAs
- DEmiRNAs, differential expression miRNAs
- AMH, antimullerian hormone

## ■ REFERENCES

- (1) Chon, S. J.; Umair, Z.; Yoon, M. S. Premature Ovarian Insufficiency: Past, Present, and Future. *Front. Cell Dev. Biol.* **2021**, *9*, 672890.
- (2) Ishizuka, B. Current Understanding of the Etiology, Symptomatology, and Treatment Options in Premature Ovarian Insufficiency (POI). *Front. Endocrinol.* **2021**, *12*, 626924.
- (3) Kovanci, E.; Schutt, A. K. Premature ovarian failure: clinical presentation and treatment. *Obstet Gynecol Clin North Am.* **2015**, *42* (1), 153–161.
- (4) McGlacken-Byrne, S. M.; Conway, G. S. Premature ovarian insufficiency. *Best Pract. Res. Clin. Obstet. Gynaecol.* **2022**, *81*, 98–110.
- (5) Li, Y.; Yan, M.; Chen, Q.; Xie, Y.; Li, C.; Han, F. Current Research on Complementary and Alternative Medicine in the Treatment of Premature Ovarian Failure: An Update Review. *Evidence-Based Complementary Altern. Med.* **2022**, *2022*, 2574438.
- (6) Jo, J.; Lee, Y. J.; Lee, H. Effectiveness of Acupuncture for Primary Ovarian Insufficiency: A Systematic Review and Meta-Analysis. *Evidence-Based Complementary Altern. Med.* **2015**, *2015*, 842180.
- (7) Li, H.; Shen, Q.; Chen, W.; Chen, W.; Feng, Z.; Yu, L. Efficacy of Traditional Chinese Medicine Tonifying Kidney (Bushen) and Activating Blood (Huoxue) Prescription for Premature Ovarian Insufficiency: A Systematic Review and Meta-Analysis. *Evidence-Based Complementary Altern. Med.* **2020**, *2020*, 1789304.
- (8) Yin, Z.; Zhang, Y. Clinical observation of Yiwei Decoction in the treatment of early onset ovarian insufficiency. *Pract. Tradit. Chin. Intern. Med.* **2022**, *36* (02), 67–69.
- (9) Guo, J.; Zhang, Y.; Tan, W. Effect of Yiwei Decoction on ultrastructure of ovarian granulosa cells in early aged female rats. *J. Chengdu Univ. Tradit. Chin. Med.* **2008**, *31* (4), 48–51.

- (10) Wu, Y.; Li, Y.; Zhang, Y.; Tan, W. Experimental study on the neuroendocrine effect of supplementing the tonic Qi of Yangming Dynasty on female primordial rat. *Chin J. Basic Med. Tradit Chin Med.* **2007**, *136* (12), 922–923.
- (11) Li, S.; Lei, Z.; Sun, T. The role of microRNAs in neurodegenerative diseases: a review. *Cell Biol. Toxicol.* **2023**, *39* (1), 53–83.
- (12) Nouri, N.; Shareghi-Oskoue, O.; Aghebati-Maleki, L.; Danaii, S.; Ahmadian Heris, J.; Soltani-Zangbar, M. S.; Kamrani, A.; Yousefi, M. Role of miRNAs interference on ovarian functions and premature ovarian failure. *Cell Commun. Signal.* **2022**, *20* (1), 198.
- (13) Yucebilgin, M. S.; Terek, M. C.; Ozsaran, A.; Akercan, F.; Zekioglu, O.; Isik, E.; Erhan, Y. Comparative study on three methods of modeling in rats with premature ovarian failure. *Chin. J. Integr. Tradit. West. Med.* **2022**, *42* (10), 1225–1230.
- (14) Kim, D.; Langmead, B.; Salzberg, S. L. HISAT: a fast spliced aligner with low memory requirements. *Nat. Methods* **2015**, *12* (4), 357–360.
- (15) Pertea, M.; Pertea, G. M.; Antonescu, C. M.; Chang, T. C.; Mendell, J. T.; Salzberg, S. L. StringTie enables improved reconstruction of a transcriptome from RNA-seq reads. *Nat. Biotechnol.* **2015**, *33* (3), 290–295.
- (16) Li, B.; Dewey, C. N. RSEM: accurate transcript quantification from RNA-Seq data with or without a reference genome. *BMC Bioinf.* **2011**, *12*, 323.
- (17) Love, M. I.; Huber, W.; Anders, S. Moderated estimation of fold change and dispersion for RNA-seq data with DESeq2. *Genome Biol.* **2014**, *15* (12), 550.
- (18) Wei, J.; Chen, T.; Liu, Y.; Sun, S.; Yuan, Z.; Zhang, Y.; Xiong, A.; Li, L.; Wang, Z.; Yang, L. Targeted bile acids metabolomics in cholesterol gallbladder polyps and gallstones: From analytical method development towards application to clinical samples. *J. Pharm. Anal.* **2023**, *13* (9), 1080–1087.
- (19) Zhou, Y.; Dai, Z.; Deng, K.; Wang, Y.; Ying, J.; Chu, D.; Zhou, J.; Tang, C. Eight Zhes Decoction ameliorates the lipid dysfunction of nonalcoholic fatty liver disease using integrated lipidomics, network pharmacology and pharmacokinetics. *J. Pharm. Anal.* **2023**, *13* (9), 1058–1069.
- (20) Zhu, L.; Yang, X.; Yao, Z.; Wang, Z.; Lai, Y.; Xu, S.; Liu, K.; Zhao, B. Bioinformatic Analysis of lncRNA Mediated CeRNA Network in Intestinal Ischemia/Reperfusion Injury. *J. Surg. Res.* **2023**, *284*, 280–289.
- (21) Li, Y.; Liu, X.; Zhang, W.; Song, X.; Zhang, L.; Xiao, C. Differently Expressed Circular RNAs in Lacrimal Sacs From Patients With Chronic Dacryocystitis. *Front. Genet.* **2022**, *13*, 834111.
- (22) Xu, L.; Liu, Y.; Wu, H.; Wu, H.; Liu, X.; Zhou, A. Rapid identification of chemical profile in Gandou decoction by UPLC-Q-TOF-MSE coupled with novel informatics UNIFI platform. *J. Pharm. Anal.* **2020**, *10* (1), 35–48.
- (23) Piątczak, E.; Kuźma, Ł.; Porada, W.; Olas, B.; Wysokińska, H. Evaluation of antioxidant properties of methanolic extracts from leaves and roots of *rehmannia glutinosa* libosch. *Acta Pol. Pharm.* **2015**, *72* (4), 777–783.
- (24) Jiang, N.; Zhao, Z. Intestinal aging is alleviated by uridine via regulating inflammation and oxidative stress in vivo and in vitro. *Cell Cycle* **2022**, *21* (14), 1519–1531.
- (25) Liang, Q.; Yang, J.; He, J.; Chen, X.; Zhang, H.; Jia, M.; Liu, K.; Jia, C.; Pan, Y.; Wei, J. Stigmasterol alleviates cerebral ischemia/reperfusion injury by attenuating inflammation and improving antioxidant defenses in rats. *Biosci. Rep.* **2020**, *40* (4), BSR20192133.
- (26) Qi, W.; Qi, W.; Xiong, D.; Long, M. Quercetin: Its Antioxidant Mechanism, Antibacterial Properties and Potential Application in Prevention and Control of Toxipathy. *Molecules* **2022**, *27* (19), 6545.
- (27) Bhattacharjee, B.; Pal, P. K.; Chattopadhyay, A.; Bandyopadhyay, D. Oleic acid protects against cadmium induced cardiac and hepatic tissue injury in male Wistar rats: A mechanistic study. *Life Sci.* **2020**, *244*, 117324.
- (28) Czerniewicz, P.; Sytykiewicz, H.; Durak, R.; Borowiak-Sobkowiak, B.; Chrzanowski, G. Role of phenolic compounds during antioxidative responses of winter triticale to aphid and beetle attack. *Plant Physiol. Biochem.* **2017**, *118*, 529–540.
- (29) Zhang, H.; Wang, Z.; Li, Z.; Wang, K.; Kong, B.; Chen, Q. l-glycine and l-glutamic acid protect *Pediococcus pentosaceus* R1 against oxidative damage induced by hydrogen peroxide. *Food Microbiol.* **2022**, *101*, 103897.
- (30) Allam, M. A. M.; Khowailed, A. A.; Elattar, S.; Mahmoud, A. M. Umbelliferone ameliorates oxidative stress and testicular injury, improves steroidogenesis and upregulates peroxisome proliferator-activated receptor gamma in type 2 diabetic rats. *J. Pharm. Pharmacol.* **2022**, *74* (4), 573–584.
- (31) Wan, M. L. Y.; Turner, P. C.; Co, V. A.; Wang, M. F.; Amiri, K. M. A.; El-Nezami, H. Schisandrin A protects intestinal epithelial cells from deoxynivalenol-induced cytotoxicity, oxidative damage and inflammation. *Sci. Rep.* **2019**, *9* (1), 19173.
- (32) Meng, Z.; Lu, J.; Ge, G.; Wang, G.; Zhang, R.; Li, Y.; Guan, S.; Lu, J. Ginsenoside Rb1 induces autophagic lipid degradation via miR-128 targeting TFEB. *Food Funct.* **2023**, *14* (1), 240–249.
- (33) Li, Z.; Rong, Y. L.; Zhang, Y. S. MiR-33–5p alleviates spinal cord injury in rats and protects PC12 cells from lipopolysaccharide-induced apoptosis. *Kaohsiung J. Med. Sci.* **2023**, *39* (1), 52–60.
- (34) Yang, Z.; An, Y.; Wang, N.; Dong, X.; Kang, H. LINC02595 promotes tumor progression in colorectal cancer by inhibiting miR-203b-3p activity and facilitating BCL2L1 expression. *J. Cell. Physiol.* **2020**, *235* (10), 7449–7464.
- (35) Sun, C.; Li, S.; Yang, C.; Xi, Y.; Wang, L.; Zhang, F.; Li, D. MicroRNA-187–3p mitigates non-small cell lung cancer (NSCLC) development through down-regulation of BCL6. *Biochem. Biophys. Res. Commun.* **2016**, *471* (1), 82.
- (36) Zhu, X.; Liu, M.; Dong, R.; Gao, L.; Hu, J.; Zhang, X.; Wu, X.; Fan, B.; Chen, C.; Xu, W. Mechanism Exploration of Environmental Pollutants on Premature Ovarian Insufficiency: a Systematic Review and Meta-analysis. *Reprod. Sci.* **2024**, *31* (1), 99–106.
- (37) Hu, Y. Y.; Zhong, R. H.; Guo, X. J.; Li, G. T.; Zhou, J. Y.; Yang, W. J.; Ren, B. T.; Zhu, Y. Jinfeng pills ameliorate premature ovarian insufficiency induced by cyclophosphamide in rats and correlate to modulating IL-17A/IL-6 axis and MEK/ERK signals. *J. Ethnopharmacol.* **2023**, *307*, 116242.
- (38) Mantawy, E. M.; Said, R. S.; Abdel-Aziz, A. K. Mechanistic approach of the inhibitory effect of chrysin on inflammatory and apoptotic events implicated in radiation-induced premature ovarian failure: Emphasis on TGF- $\beta$ /MAPKs signaling pathway. *Biomed. Pharmacother.* **2019**, *109*, 293–303.
- (39) Said, R. S.; El-Demerdash, E.; Nada, A. S.; Kamal, M. M. Resveratrol inhibits inflammatory signaling implicated in ionizing radiation-induced premature ovarian failure through antagonistic crosstalk between silencing information regulator 1 (SIRT1) and poly(ADP-ribose) polymerase 1 (PARP-1). *Biochem. Pharmacol.* **2016**, *103*, 140–150.
- (40) Lei, K.; Wei, Q.; Cheng, Y.; Wang, Z.; Wu, H.; Zhao, F.; Ding, W.; Shi, F. OONO-/MMP2/MMP9 pathway-mediated apoptosis of porcine granulosa cells is associated with DNA damage. *Reproduction* **2023**, *165* (4), 431–443.
- (41) Portela, V. M.; Veiga, A.; Price, C. A. Regulation of MMP2 and MMP9 metalloproteinases by FSH and growth factors in bovine granulosa cells. *Genet. Mol. Biol.* **2009**, *32* (3), 516–520.
- (42) Li, S.; Liu, M.; Ma, H.; Jin, Q.; Ma, Y.; Wang, C.; Ren, J.; Liu, G.; Dai, Y. Ameliorative effect of recombinant human lactoferrin on the premature ovarian failure in rats after cyclophosphamide treatments. *J. Ovarian Res.* **2021**, *14* (1), 17.
- (43) Abogresha, N. M.; Mohammed, S. S.; Hosny, M. M.; Abdallah, H. Y.; Gadallah, A. M.; Greish, S. M. Diosmin Mitigates Cyclophosphamide Induced Premature Ovarian Insufficiency in Rat Model. *Int. J. Mol. Sci.* **2021**, *22* (6), 3044.
- (44) Qu, L.; Liu, Y.; Deng, J.; Ma, X.; Fan, D. Ginsenoside Rk3 is a novel PI3K/AKT-targeting therapeutics agent that regulates autophagy and apoptosis in hepatocellular carcinoma. *J. Pharm. Anal.* **2023**, *13* (5), 463–482.

- (45) Rak, A.; Drwal, E.; Wróbel, A.; Gregoraszczyk, E. L. Resistin is a survival factor for porcine ovarian follicular cells. *Reproduction* **2015**, *150* (4), 343–355.
- (46) Oriá, R. B.; de Almeida, J. Z.; Moreira, C. N.; Guerrant, R. L.; Figueiredo, J. R.; Apolipoprotein, E. Apolipoprotein E Effects on Mammalian Ovarian Steroidogenesis and Human Fertility. *Trends Endocrinol. Metab.* **2020**, *31* (11), 872–883.
- (47) Sakurai, M.; Ohtake, J.; Ishikawa, T.; Tanemura, K.; Hoshino, Y.; Arima, T.; Sato, E. Distribution and Y397 phosphorylation of focal adhesion kinase on follicular development in the mouse ovary. *Cell Tissue Res.* **2012**, *347* (2), 457–465.
- (48) Walter, J.; Monthoux, C.; Fortes, C.; Grossmann, J.; Roschitzki, B.; Meili, T.; Riond, B.; Hofmann-Lehmann, R.; Naegeli, H.; Bleul, U. The bovine cumulus proteome is influenced by maturation condition and maturational competence of the oocyte. *Sci. Rep.* **2020**, *10* (1), 9880.
- (49) Sun, T.; Xiao, C.; Yang, Z.; Deng, J.; Yang, X. Grade follicles transcriptional profiling analysis in different laying stages in chicken. *BMC Genom.* **2022**, *23* (1), 492.
- (50) Wang, X.; Zhao, N.; Wang, T.; Du, S.; Liu, Q.; Li, J. Transcriptome Analysis Provides Insights into Copulation, Fertilization, and Gestation in *Sebastes schlegelii*. *Genes* **2022**, *13* (10), 1812.
- (51) Skinner, M. K.; Schmidt, M.; Savenkova, M. I.; Sadler-Riggelman, I.; Nilsson, E. E. Regulation of granulosa and theca cell transcriptomes during ovarian antral follicle development. *Mol. Reprod. Dev.* **2008**, *75* (9), 1457–1472.
- (52) Lee, H. J.; Cho, C. H.; Hwang, S. J.; Choi, H. H.; Kim, K. T.; Ahn, S. Y.; Kim, J. H.; Oh, J. L.; Lee, G. M.; Koh, G. Y. Biological characterization of angiotensin-3 and angiotensin-4. *FASEB J.* **2004**, *18* (11), 1200–1208.
- (53) Jung, J. H.; Kim, J. H.; Song, G. G.; Choi, S. J. Association of the F13A1 Val34Leu polymorphism and recurrent pregnancy loss: A meta-analysis. *Eur. J. Obstet. Gynecol. Reprod. Biol.* **2017**, *215*, 234–240.
- (54) Pei, J.; Song, R.; Bao, P.; Yin, M.; Li, J.; Zhang, G.; Wu, F.; Luo, Z.; Wu, X.; Song, W.; Ba, Y.; Xiong, L.; Liang, C.; Guo, X.; Yan, P. Differential proteomic analysis demonstrates follicle fluid participate immune reaction and protein translation in yak. *BMC Vet. Res.* **2022**, *18* (1), 34.
- (55) Sun, Z.; Wang, Y.; Wei, T.; Liu, L. Identification of key genes and miRNAs related to polycystic ovary syndrome by comprehensive analysis of microarray. *BMC Med. Genom.* **2022**, *15* (1), 267.
- (56) Sha, Y.; Liu, W.; Tang, S.; Zhang, X.; Xiao, Z.; Xiao, Y.; Deng, H.; Zhou, H.; Wei, X. TENT5D disruption causes oligoasthenoteratozoospermia and male infertility. *Andrology* **2023**, *11* (6), 1121–1131.
- (57) Cong, J.; Yang, Y.; Wang, X.; Shen, Y.; Qi, H. T.; Liu, C.; Tang, S.; Wu, S.; Tian, S.; Zhou, Y.; He, X.; Wang, L.; Liu, M. F.; Zhang, F. Deficiency of X-linked TENT5D causes male infertility by disrupting the mRNA stability during spermatogenesis. *Cell Discovery* **2022**, *8* (1), 23.